RESEARCH

Exploring the stability of single emulsion created by microfluidics and its use in the production of core–shell microparticles

Mehrnaz Oveysi[1] · Vahid Bazargan[1] · Amir Nejat[1] · Marco Marengo[2]

Abstract

This study introduces an innovative method aimed at achieving exceptional stability in emulsions. The primary focus is on re-emulsifying precisely controlled and uniform initial single emulsions, generated by microfluidic devices, to produce single-core double emulsions and core–shell microparticles. Departing from traditional approaches, our method employs a unique combination of advanced Two-level fractional factorial design and numerical simulation. These tools are utilized to discern and optimize critical parameters necessary for the formation of highly monodispersed stable single emulsions and their subsequent transformation into double emulsions. Correlations are established to estimate the size and stability of the primary single emulsion based on immiscible phase flow rate ratio and surfactant concentration. These correlations provide a comprehensive understanding that facilitates the intentional development of desired water-in-oil emulsions. The proposed microfluidic paradigm shows promise for the controlled and efficient production of single-core double emulsions, with broad applications in Pharmaceuticals, Food, and Cosmetics.

1 Introduction

Water-in-oil (w/o) emulsions have been commonly produced utilizing microfluidic devices. Leveraging minimal energy consumption and precise process control, microfluidic emulsification presents a compelling avenue for diverse applications Sahin et al. (2016). The notable advantage of employing a microfluidic droplet generator is the attainment of monodispersity in the resulting emulsion. Consequently, a crucial inquiry arises regarding the preservation of this monodispersity over time, namely, the stability of the emulsion. Although (w/o) emulsions play a crucial role in industries such as food and pharmaceuticals, their stability poses a significant challenge (Zembyla et al. 2020; Colucci et al. 2020). The stability of an emulsion against coalescence is considered to be affected by drop volume fraction, the size distribution of drops, the flow conditions Ho et al. (2022),

type and concentration of surfactants Zhang et al. (2020), droplet size and size variation El Bouchikhi et al. (2021), salinity and viscosity Goodarzi and Zendehboudi (2019). The successful creation of a stable emulsion formulation in a microfluidic device requires the careful selection of numerous excipients, including emulsifiers and all the previously listed parameters. Micron-sized droplets are stabilized by the presence of a surfactant that is soluble in the continuous phase, as commonly observed empirically Zdrali et al. (2019). Bacteria in (w/o) emulsion improved droplet stability, and a greater number of dead cells enhanced stability by having a strong attraction to the interface Mohd Isa et al. (2022). Zhang et al. (2023) showed soy emulsions made using microfluidics exhibited better oxidative stability than those made using homogenizers. Emulsions were temperature, pH, and salt ion stable (Francisco et al. 2022; Jayakumar et al. 2023). Under controlled conditions, flow-focusing device-produced emulsions stabilized with different dairy protein concentrations were compared. To comprehensively understand the interplay of these factors and their impact on emulsion outcomes, a high-dimensional experimental design approach can be used Sanchez et al. (2020). There are various instances of how experimental design has been

✉ Vahid Bazargan
vbazargan@ut.ac.ir

[1] School of Mechanical Engineering, College of Engineering, University of Tehran, Tehran, Iran

[2] Department of Civil Engineering and Architecture, Faculty of Engineering, University of Pavia, Pavia, Italy

used to develop or improve emulsion formulations (Abdul-redha et al. 2019; Raya et al. 2022; BenJemaa et al. 2022).

Experimental and numerical approaches have been successfully employed for analyzing two-phase flows, predicting droplet formation regime, diameter, monodispersity, and production rate in widespread flow-focusing devices (Yu et al. 2019; Sontti and Atta 2019; Filimonov et al. 2021; Soroor et al. 2021; Liu et al. 2021). These studies have considered factors such as the flow rate ratio of the dispersed and continuous phases, surfactant concentrations, device geometry, and phase viscosities, all of which influence droplet diameter and monodispersity in planar microfluidic devices (Wu et al. 2019; Paiboon et al. 2022; Chagot et al. 2022). Despite the progress made through numerical simulations to study droplet formation behavior, experimental research is still essential to explore key aspects such as the emulsion stability or the effect of surfactant type on droplet formation behavior.

This study aims to bridge the gap between microfluidic emulsion formation and the long-term stability of highly monodispersed single water-in-oil (w/o) emulsions. By employing a numerical level-set approach, we predicted specific conditions for achieving a highly uniform emulsion. Our investigation delves into how changes in interfacial tension and flow rate ratios impact droplet formation and single emulsion sizes. The innovative fusion of a two-level fractional factorial design and numerical simulations aims to uncover insights into critical parameters influencing stable and consistently sized single water-in-oil emulsions, minimizing the need for extensive trial-and-error experiments. Moreover, we take a step further by re-emulsifying the single emulsion to create single-core double emulsions, following the method described by Wang et al. (2022). After producing highly monodispersed stable single (w/o) emulsion of desired size, the utilization of a vortex mixer to re-emulsify the single (w/o) emulsion, provides a straightforward and efficient approach for generating water-in-oil-in-water (w/o/w) double emulsions through shear force. We explore the relationship between the stability of the single emulsion and the uniformity and size of the double emulsion. The practical application of our study is demonstrated by producing exceptionally homogeneous polymeric core-shell microparticles with the incorporation of PLGA as a crucial element in forming the shell of core-shell particles.

2 Materials and methods

2.1 Materials

The microfluidic device was made using Polydimethyl-siloxane (PDMS, Sylgard 184), and was purchased from

Table 1 Properties of continuous (oil) and dispersed Phase (water) for each sample

Surfactant Type	Sample 1	Sample 2	Sample 3	Sample 4
Span 80 concentration in continuous (oil) phase (wt%)	2%	0%	0%	2%
SDS concentration in dispersed (water) phase (wt%)	0%	0.3%	0%	0.3%

Table 2 Physical properties of all fluids used in the experiment

Sample solution	Viscosity (mPa.s)	Density(gr/cm^3)
Mineral oil	22.2	0.87
Dichloromethane	0.4	1.33
Continuous phase (Sample 1–4)	3.77	1.1
Dispersed phase (Sample 1–4)	1.1	0.9

Dow Corning(Michigan, USA), along with a curing agent. The microdevice was built using a protocol that had already been disclosed elsewhere Oveysi et al. (2023). We sourced PLGA 75:25 (poly(lactide-co-glycolide), M_w 66,000–107,000), Dichloromethane (DCM), Mineral oil, as well as the anionic emulsifiers Span 80 and Sodium dodecyl sulfate (SDS) from Sigma Aldrich Chemicals.

A solution was prepared by dissolving 1 wt% PLGA in dichloromethane. The combination is dissolved in mineral oil at a volume-to-volume ratio of 0.5, resulting in the continuous phase. For enhanced visibility, we locally procured yellow food dye, which was incorporated at a concentration of 0.1 wt% in the aqueous phase (deionized water). The dispersed phase is created by adding varying concentrations of SDS to this aqueous solution. Different concentrations of Span 80 and SDS are added to the continuous and dispersed phases. The four samples that are required for our experiments are listed in Table 1. The rotational rheometer from TA Instruments is employed to measure the viscosities of both the dispersed and continuous phases. The data shows that both phases exhibit Newtonian behaviour over the whole range of shear rates, with dynamic viscosities of 1.1 mPa-s and 21.9 mPa-s for the dispersed and continuous phases, respectively. The readings exhibited uniformity across all four samples and did not display substantial fluctuations at different levels of surfactant concentration, which may be attributed to the lack of micelle formation. The level of inaccuracy was

found to be approximately ± 0.05 mPa s. Table 2 lists the physical properties of all fluids used in the experiments.

2.2 Interfacial tension versus surfactant concentration

Jikan CAG-20, an automatic device for measuring static and dynamic contact angles, and surface and interfacial tensions, was used to measure interfacial tension between the two phases at room temperature. Measurements of interfacial tension are essential for specifying the materials used in the numerical study. The magnitudes of the interfacial tension are measured and listed in Table 3. As anticipated, the inclusion of surfactant in either the water or oil phases or both of them results in the observation of a reduction of the interfacial tension. To quantify the interfacial tension of the materials under investigation, we conducted a comprehensive experimental study. Our approach involved varying the surfactant (SDS) concentration in the aqueous phase from 0 to 0.3 while adjusting the Span 80 concentration in the oil phase across a range from 0 to 2. Through systematic experimentation and data collection across these concentration gradients, we aimed to elucidate the influence of surfactant concentrations on interfacial tension.We identified specific combinations of SDS and Span 80 concentrations that yielded nearly identical interfacial tension values for both samples. We chose the surfactant concentration in either phase so that the interfacial tension between case 1, which is surfactant-laden oil and pure water, and case 2, which is surfactant-laden water and pure oil, is the same. The purpose of this method was to evaluate the numerical simulation quality when a surfactant is introduced in the dispersed phase, which is less common than introducing it in the continuous phase Chen et al. (2020).

It is important to note that the interfacial tension was measured using an instrument with a standard deviation of 0.1 mN/m. When comparing samples containing water with a nominal surfactant (SDS) concentration of 0.01wt% to those without added surfactant, it was observed that the measured interfacial tension values for both scenarios appeared to be identical and potentially fell within the margin of error of the device.

Notably, the concentrations in our study were deliberately kept below the critical micelle concentration (CMC),

where surfactant molecules transition from adsorbing at the interface to form aggregates in bulk. Beyond the CMC, increasing the emulsifier concentration does not lead to a further decrease in interfacial tension, as the concentration of the surfactant layer at the interface reaches its maximum value Ho et al. (2022). In water, the CMC value of SDS is reported to be 0.23−0.43 wt% (Chatterjee et al. 2001; Issakhani et al. 2023) and in mineral oil, the CMC of the oil phase is reported to be (0.05wt%) Narayan et al. (2020). The CMC of the dispersed phase was determined to be 0.35 wt%, whereas the continuous phase exhibited a CMC of 2.2 wt%. The values were obtained by identifying the threshold at which increasing the surfactant concentration ceased to affect the interfacial tension. The difference in the CMC value of Span 80 in the oil phase, as compared to the value reported in the literature, can be explained by the presence of Poly(lactic-co-glycolic acid) (PLGA) in the oil phase Kumar et al. (2013).

2.3 Experimental

2.3.1 Microfluidic generation of droplets

The two phases, the water phase, and the oil phase, were injected into the microfluidic chip as shown in Fig. 1 via tubes using a syringe pump (Harvard PHD) at the designated flow rate. The dispersed phase (Q_d) consisted of the aqueous phase with or without surfactant addition, while the continuous phase (Q_c) comprised a surfactant-laden or pure oil phase. The formation of water droplets occurred at the junction of the microfluidic flow-focusing chip. The microfluidic droplet generator's minimum feature size, specifically the orifice (W_d), was 30 µm. The dimensions of the outlet channel, both the side channels and the main channel (W_I) were 100 µm wide. A constant depth (H) of 100 µm was maintained across all channels. The emulsion was collected in a 1.5 mL microtube containing 500 µL mineral oil, using a PTFE tube with an inner diameter of 0.76 mm and an outer diameter of 2 mm. The process of visualization was facilitated by employing the Pixelink camera (Model Number: PL-D7912CU-T) which is mounted on the Olympus IMT-2 inverted fluorescent microscope. In the collection container, stability against coalescence is tested two weeks after emulsion formation. The research employed a two-level fractional factorial design methodology to evaluate the statistical relevance of the flow rate ratio and surfactant concentration in each phase on the stability of the emulsion, which exhibited a high degree of monodispersity following its formation. A total of eight experimental designs were generated using the formula $2^{(K)}$, where K represents the number of factors in the experiment Ait-Amir et al. (2020). Eight experiments with zero center points were conducted with three independent variables, denoted as (A), (B), and (C), each varying at

Table 3 Interfacial tension between the continuous and dispersed phase for each sample used in this Study at 25 °C with a standard deviation of 0.1 mN/m

Emulsion	Sample 1	Sample 2	Sample 3	Sample 4
Interfacial Tension (mN/m)	4.8	4.8	30.5	1.7

Fig. 1 Single emulsion creation in a microfluidic device is depicted schematically. (1) Aqueous (dispersed) phase inlet, (2) Oil (continuous) phase inlets, (3) PTFE collection tube, (4) Collection tank containing 5 ml mineral oil
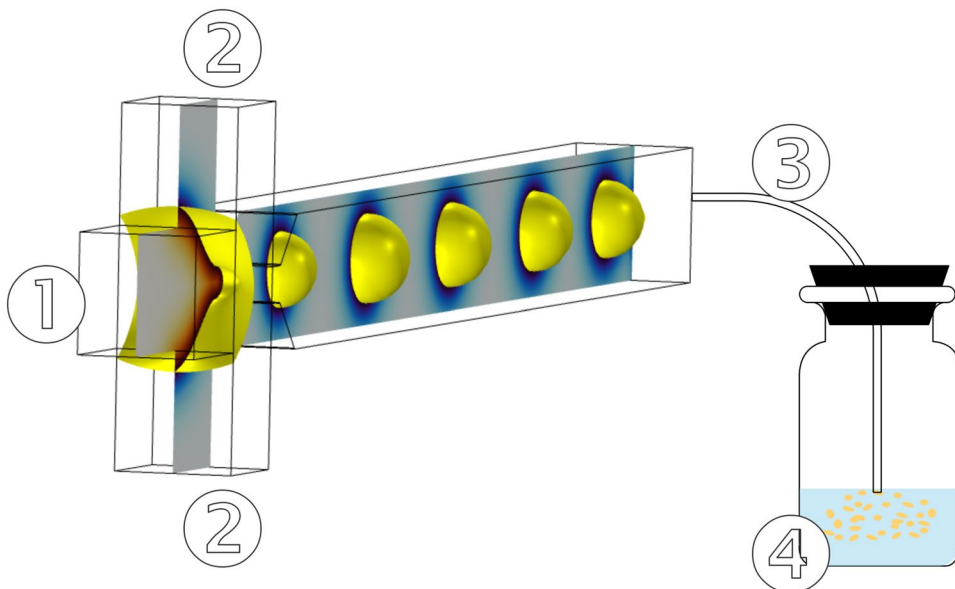

Table 4 Independent variables of fractional factorial design

Parameters	Factor level	Coded level (-1)	Coded level (+1)
Surfactant concentration (SDS) in water phase	A	0%	0.3%
Surfactant (Span 80) concentration in oil phase	B	0%	2%
Flow rate ratio	C	1	5

two levels within the coded range from -1 to +1, as demonstrated in Table 4. The determination of the range of levels is accomplished through the implementation of a numerical simulation, which serves to comprehensively delineate the behavior of droplet formation. It is critical to recognize that the ranges are established in such a way that droplets can form in the squeezing regime. The squeezing regime was

chosen because of its proven track record of producing droplet production that is regularly and uniformly dispersed, outperforming other regimes in this regard Mahdi et al. (2017). In our study, we have centered our stability assessment on emulsions with a remarkably uniform droplet size distribution, characterized by a coefficient of variation (CV) of less than 5%. Through meticulous control over the microfluidic generation of the emulsion, guided by our numerical results, we have effectively eliminated fluctuations in droplet size (polydispersity). Therefore, we have been able to study the effect of working parameters on the stability of the highly monodispersed emulsion. To determine whether influences are statistically significant on response, the experimental findings are examined using Minitab statistical software, which generates normal probability plots. A fitted model outlining how variables affect stability was also offered.

2.3.2 Core-shell PLGA microparticle fabrication

As shown in Fig. 2, to generate a double emulsion, a single emulsion that is produced in a microfluidic droplet generator

Fig. 2 Generation of double emulsion via laboratory vortex. The monodispersed single emulsion created by microfluidics was collected in a microtube, and then an aqueous phase was introduced. In the re-emulsification process, single-core double emulsions are created by vortexing for the required duration
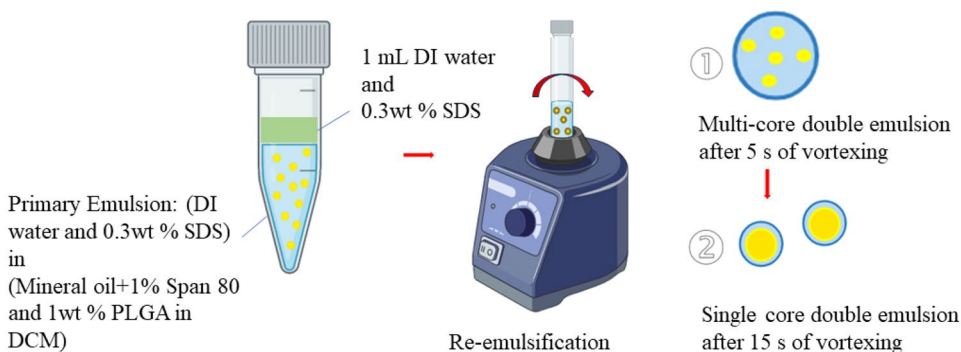
was collected in a microtube. The concentration of Span 80 and SDS added to generate a single emulsion is calculated using the correlation that is obtained in this study to achieve the highest stability. The single emulsion is transferred to a 1 mL aqueous phase containing 0.3 weight percent sodium dodecyl sulfate (SDS) and vortexed for 15 s at room temperature at a rotational speed of 2000 revolutions per minute, based on Wang et al. (2022) findings. According to this study, during the initial stages of vortexing, the agitation causes the formation of oil droplets that encapsulate several core (water) droplets. The process of repeated vortexing of the container causes the large oil droplets to be broken down into smaller droplets, resulting in each droplet containing only one water core. This fragmentation process is facilitated by the combined influence of shear and centrifugal forces, ultimately resulting in each droplet encapsulating a single water core. These core droplets have a consistent size that is the same as the primary emulsion.

The double emulsion is stirred on a magnetic stirrer for 16 h to evaporate DCM to create microparticles. To eliminate any remaining SDS, the microparticles were rinsed thrice with DI water.

2.4 Numerical modeling of single droplet formation

2.4.1 Governing equations

In numerical analysis and to observe the interface between immiscible fluids, it is necessary to solve the continuity equation (Eq. 1), momentum equation (Eq. 2), and level-set equation (Eq. 3), as stated by Mitra and Chakraborty (2012). ρ (Kg/m^3) is the density, t (s) is the time, and v is the velocity vector. p (Pa) is the pressure and μ is the viscosity. F_σ is the interfacial force per unit area at the interface of the two phases. γ (m/s) is a parameter used for re-initialization and the parameter ε (m) controls the interface thickness. The characterization of the fluid phase within the level-set method is determined by the level-set function (φ), which is a function dependent on both spatial coordinates and temporal evolution. The fluid properties, specifically the volume-averaged density (Eq. 4) and viscosity (Eq. 5), are estimated using the level-set function. The geometric characteristics of a microfluidic planar cross-junction device are considered in the numerical simulation of three-dimensional droplet generation using COMSOL version 6.0. The simulations were performed using an Intel® Core™ i9-13900K processor and OCPC 32 Gb, 32,000 MHz RAM.

$$\frac{\partial}{\partial t}(\rho) + \nabla.(\rho v) = 0 \tag{1}$$

$$\frac{\partial}{\partial t}(\rho v) + \nabla.(\rho v.v) = -\nabla p + \nabla.[\mu(\nabla.v + \nabla.v^T)] + F_\sigma \tag{2}$$

$$\frac{\partial}{\partial t}(\varphi) + \nabla(v\varphi) = \gamma\nabla.\left[\varepsilon\nabla(\varphi) - \varphi(1-\varphi)\frac{\nabla(\varphi)}{|\nabla(\varphi)|}\right] \tag{3}$$

$$\rho = \rho_c + (\rho_c - \rho_d)\varphi \tag{4}$$

$$\mu = \mu_c + (\mu_c - \mu_d)\varphi \tag{5}$$

Using the continuum surface force (CSF) model of Brackbill et al. (1992), the interfacial force is reformulated as an equivalent body force (Eq. 6) acting at the interface.

$$F_\sigma = \sigma\kappa(\varphi)\delta(\varphi)\nabla(\varphi) \tag{6}$$

where σ is the fluid surface tension coefficient. $\kappa(\varphi)$ is the interface curvature defined as,

$$\kappa(\varphi) = \nabla.\frac{\nabla\varphi}{|\nabla\varphi|} \tag{7}$$

and $\delta(\varphi)$ is the smoothed Dirac delta function for which several estimations have been proposed Zhang (2014).

2.4.2 Grid convergence test

Before performing the parametric studies, a mesh sensitivity study is performed on the minimum thread length. This investigation involves using several element sizes, specifically 12, 10, 8, 6, and 4 μm. The comparison between interface evolution when different sizes of mesh are shown in Fig. 3. A grid independence test is conducted by employing five different mesh element sizes. Figure 4 illustrates the minimal width of the neck during thread break-up for droplet formation under varying mesh element sizes. It is observed that the numerical results exhibit convergence as the grid resolution increases. To ensure precision and efficiency, a mesh element size of 6 μm. The 41,132 hexahedral grids with a maximum mesh element size of 6 μm and minimum element size of 0.27 μm are systematically traversed throughout the three-dimensional domain, as depicted in Fig. 5. There are also 14,700 quads and 1512 edge elements in the customized mesh. The mesh refinement is specifically concentrated near the wall to achieve a precise representation of the thin liquid layer in the region.

2.4.3 Numerical model validation

The numerical model is initially tested using typical experimental findings of Fu et al. (2012). The comparison between our numerical simulation using the Fu et al setting as a typical validation case is shown in Fig. 6. It shows a qualitative comparison of droplet pinch-off behavior with the corresponding experimental observations of Fu et al.

Fig. 3 Comparison of interface evolution at t=0.1 (s) when maximum element size is: (1) 12 μm (2) 10 μm (3) 8 μm (4) 6 μm (5) 4 μm
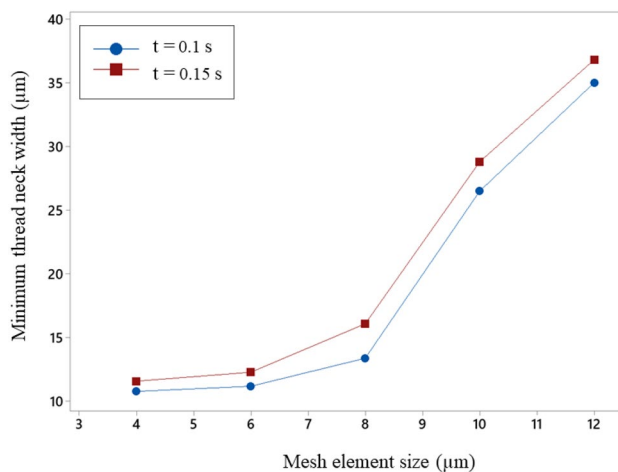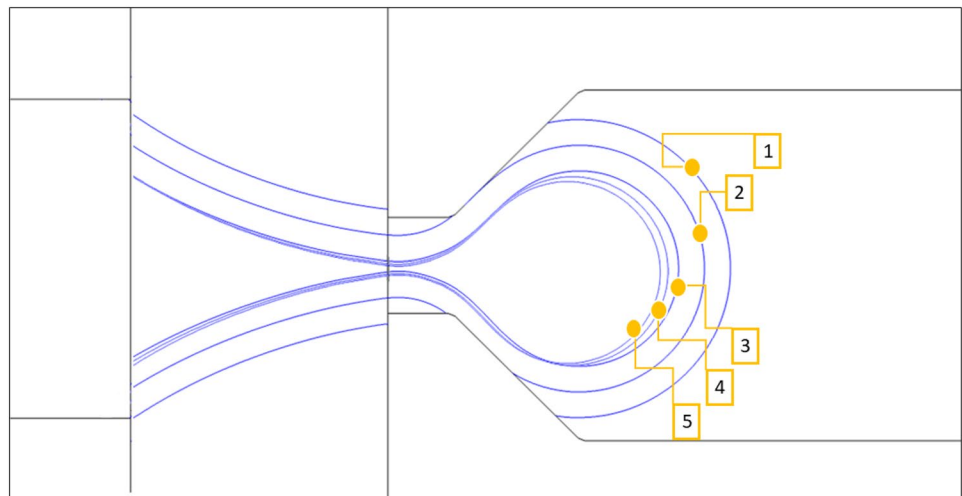

Fig. 4 Grid independence test showing minimum thread width before droplet detachment with different mesh sizes of (1) 12 μm (2) 10 μm (3) 8 μm (4) 6 μm (5) 4 μm

To further examine the numerical simulation with our experimental results, the flow rate of the dispersed (water phase) and continuous phase (oil phase) is set to 0.5 μL/min and 1 μL/min, respectively. It may be inferred from Fig. 7 that our numerical model demonstrated satisfactory capability in forecasting droplet pinch-off behavior. Further validation of the predicted droplet diameter is encompassed in subsequent sections as well.

2.4.4 Droplet size and coefficient of variation measurement

The images from the numerical simulation and experiments were analyzed using the Image-J software to determine the diameter of each droplet. The apparent diameter (D(1)) Dapčević Hadnađev et al. (2013) was determined as the median value of the droplet population distribution, which was obtained from at least 100 droplets captured from different frames.

In the numerical simulations, the number of elements with a level-set of 1 was obtained from the region encircling the droplet to calculate the diameter of a single droplet. After identifying the quantity of the aforementioned elements, the volume of the droplet was calculated by adding their volumes. Finally, the diameter ($D(1)$) can be calculated using the volume of a spherical droplet. Dimensionless diameter is calculated according to (Eq. 8).

$$\frac{D(1)}{D_H} = \left(\frac{2w_d h}{w_d + h} \right) \tag{8}$$

To assess the droplet size distribution, the coefficient of variation (CV) is computed utilizing the formula (Eq. 10):

$$CV(\%) = \left(\frac{\sigma}{\bar{D}} \right) \tag{9}$$

where,

$$\sigma = \sqrt{\frac{1}{N} \sum_{i=1}^{N} (D(1) - \bar{D})} \tag{10}$$

2.5 Single emulsion stability index measurement

To define an emulsion's stability, the proportion of droplets that did not coalesce, dubbed the stability parameter against coalescence, was employed by Chacon Orellana and Baret (2019). In the study conducted by Baret et al. (2009), the parameter p(1) (Eq. 11) is employed for on-chip measurement of droplet stability about coalescence and p(1) > 0.999, the emulsion was considered to be stable. In

Fig. 5 Computational grid depicted in three dimensions. Mesh refinement is used near the wall and orifice
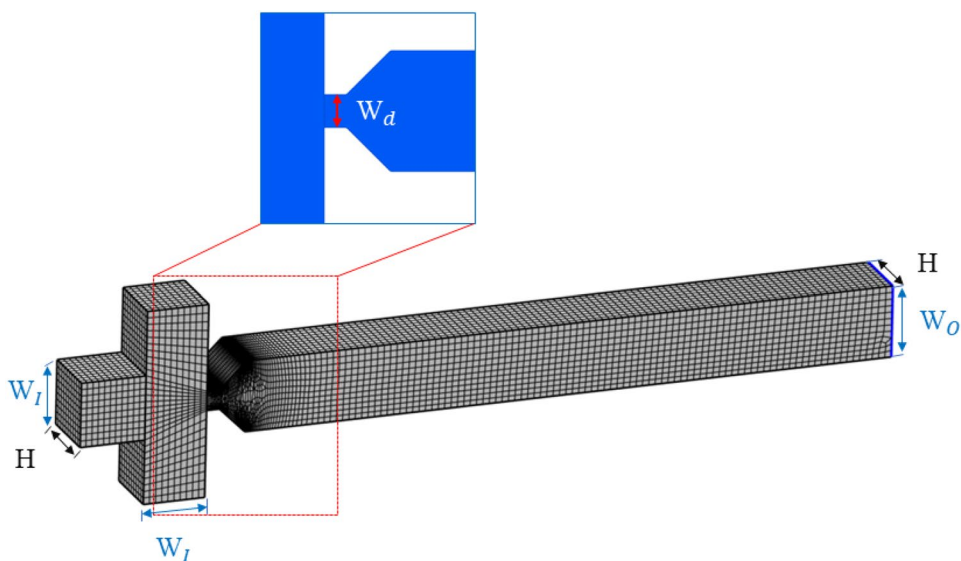
the given equation, the variable n(1) represents the number of unfused droplets, while $\Sigma in(i)$ denotes the total count of all droplets. In our work, we use (Eq. 11) to describe the emulsion collected outside of the chip.

$$\P(1) = \frac{n(1)}{\Sigma in(i)} \tag{11}$$

The emulsions are tested after 14 days of preparation to examine their resistance to merging. To determine the number of droplets in the collecting container, the frequency of droplet generation (f) was calculated using video microscopy. The number of drops created over the recorded time was calculated as the droplet generation frequency for each run (Eq. 12). Subsequently, given the duration of droplet generation run (L), we calculated the number of created droplets, that is $\Sigma in(i)$. A MATLAB algorithm is used to count the number of total droplets n(1) in an image of the collected droplets that did not change in diameter after 14 days, with a diameter of $D \pm 10\,\%D$.

$$\Sigma in(i) = L.f \tag{12}$$

3 Results and discussion

### 3.1 Numerical results: water droplet generation under varying flow rate ratios and interfacial tensions

To commence the investigation, a numerical simulation is conducted to ascertain the methodology for achieving a squeezing regime utilizing our microfluidic device. Based on our numerical analysis, we have derived a flow regime

diagram and identified the range of flow rate ratios (Q_c/Q_d) and capillary numbers for the continuous phase ($Ca = \mu v/\sigma$) necessary to achieve the squeezing regime. The relationship between droplet diameter variation and flow rate ratio, as well as the capillary number of the continuous phase, is observed. These parameters indicate the impact of the primary force involved in droplet formation. The flow rates of the dispersed phase (Q_d) and continuous phase (Q_c) are varied from 1 to 7 µL/min and 1 to 35 µL/min, respectively, to explore the influence of the flow rate ratio on droplet formation behavior.

When the water phase is combined with a surfactant (SDS) and the oil phase is pure (Sample 2), the resulting interfacial tension is found to be the same as in Sample 1 (pure water and span 80-laden oil phase), as indicated in Table 3. Therefore, our numerical simulation predicted the same droplet formation for both samples 1 and 2. To assess the accuracy of the numerical model in predicting changes in droplet diameter for Samples 1 and 2 with varying flow rate ratios, a quantitative comparison is conducted between experimental (with a 95% confidence limit) and numerical data. This comparison involves adjusting the flow rate of the continuous phase to values of 1 and 35 µL/min while maintaining a dispersed flow rate of 1 µL/min. The results presented in Fig. 8 demonstrate a satisfactory level of agreement.

Although the error in droplet diameter prediction in the numerical study is acceptable for both Sample 1 and 2, it can be concluded that the results are more precise for Sample 1 with a surfactant-laden continuous phase compared with that of Sample 2. Therefore, it is advisable to investigate the process of surfactant mass transfer to analyze the interfacial layer between the water and oil phases in this particular

Fig. 6 Comparison of droplet
generation process between
numerical simulation (on the
x-y plane) and Fu et al. (2012)
experiment in a microfluidic
cross-junction with square sec-
tions. (Scale bar: 600 μm)
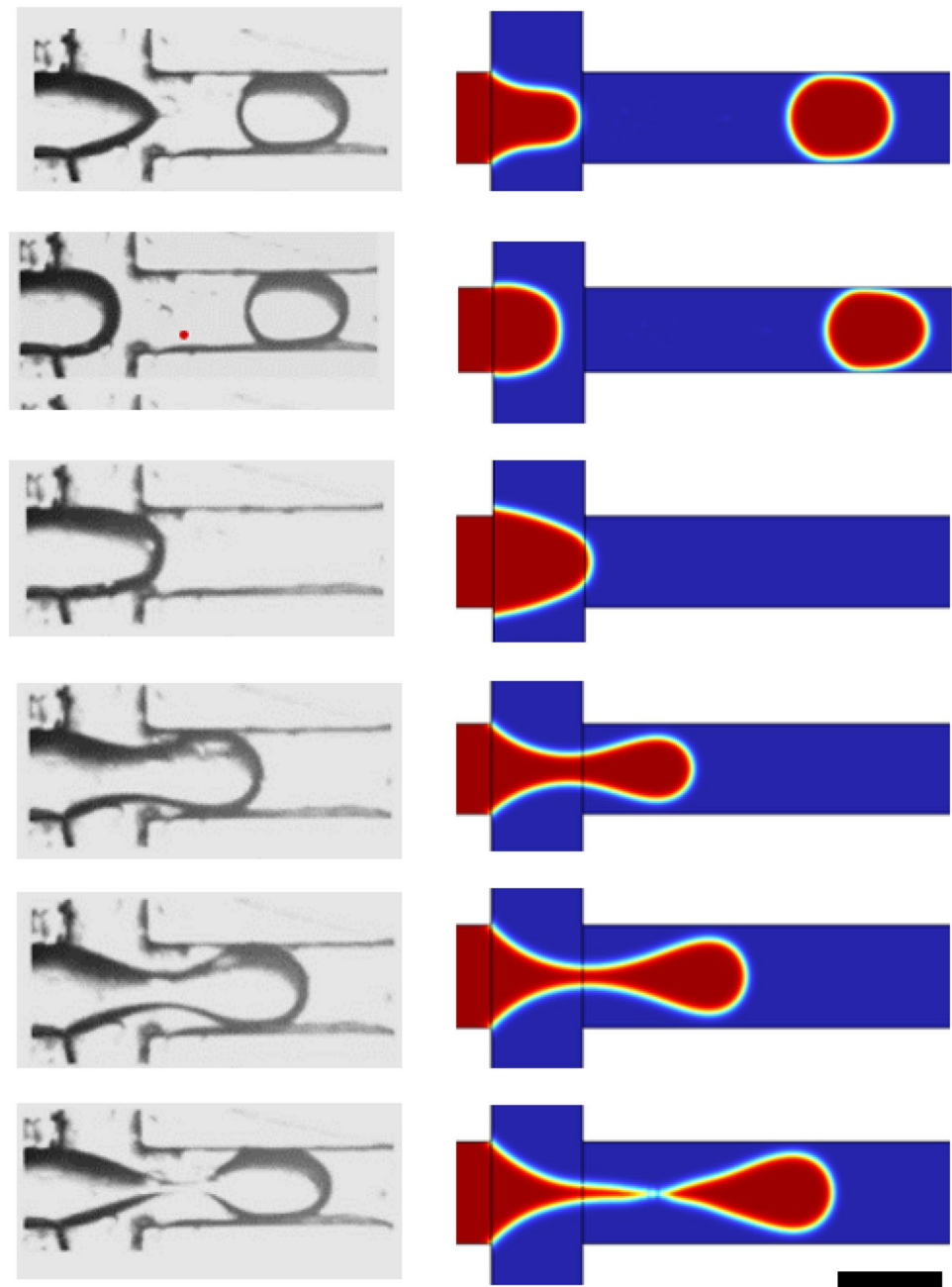
scenario, as demonstrated by Kiratzis et al. (2022), which is
beyond the scope of this study.

For Samples 1, 2, and 4, for which we have numerical
results, we generate the flow regime diagram as depicted in
Fig. 9. The shaded area in each diagram corresponds to the
selected flow rate ratio (ranging from 1 to 5) and capillary
number range (up to 0.0038 and 0.0045 for Sample 1(2) and
4, respectively). This selection ensures that we are operat-
ing within the squeezing regime of droplet formation. The
diagram also includes the dripping regime and the transition
region from dripping to the jetting regime for each sam-
ple. In both Sample 1 and Sample 2, the observed droplet

production regime across all flow rate ratios is squeez-
ing when the capillary number of the continuous phase is
smaller than 0.0038, as shown in Fig. 9a. This regime is
characterized by the retraction of the dispersed phase after
droplet formation, pressure build-up due to the dispersed
phase obstructing the channel after expanding, and a necking
stage due to squeezing pressure build-up, ultimately leading
to droplet pinch-off Yu et al. (2019). Under identical condi-
tions, all these steps are detected in both experimental and
numerical experiments of Sample 1 and 2.

The incorporation of surfactant in both phases, as
observed in Sample 4, leads to a significant reduction in

Fig. 7 The process of water droplet formation, (a-b) Expanding, (c) Necking, (d) Pinch-off was observed by experiments (top) and simulations (bottom) using the oil phase as a continuous phase. Specifically, the flow rates used were 1 μL/min and 2 μL/min for the water and oil phases, respectively. In the conducted studies, a small quantity of yellow food dye (specifically, 2 drops per 50 ml) was introduced into the dispersed phase to enhance the clarity of the resulting images (Scale bar: 50 μm)
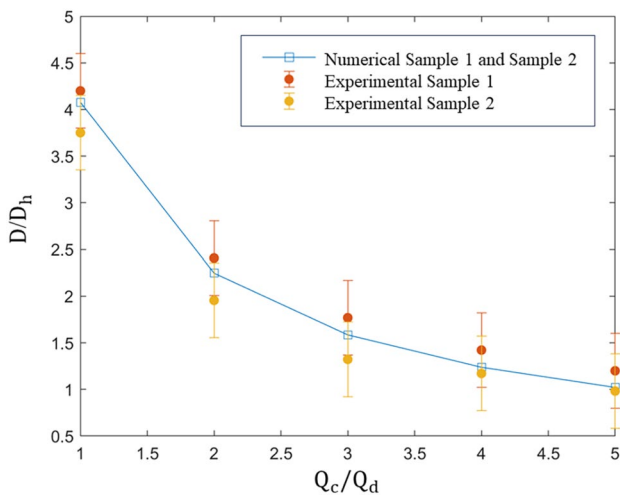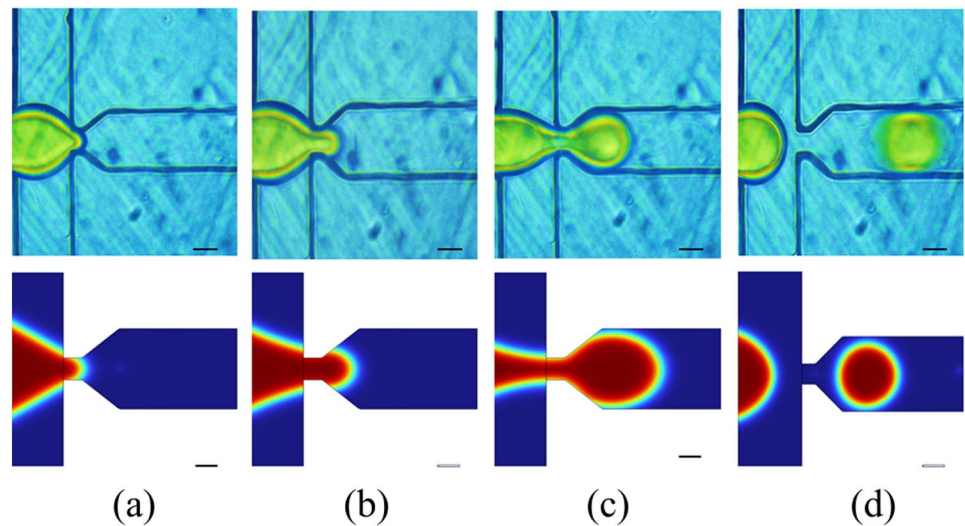

Fig. 8 The accuracy of the numerical results is assessed by conducting a comparison between the droplet diameter of Sample 1 and 2 seen at different flow rate ratios and the corresponding numerical data. The error bars reflect the standard deviation of the mean

interfacial tension to its minimal level in our study. Consequently, this results in an elevated transition capillary number from the squeezing to dripping regime, as illustrated in Fig. 9b.

In the absence of surfactant in both the oil and water phases (Sample 3), the generation of droplets is impeded, preventing the observed fragmentation of the dispersed phase at the junction, as indicated by numerical studies. The lack of numerical data for this sample is attributed to the observation of the parallel flow of the two immiscible phases in the conducted numerical investigation.

Figure 10a, b illustrate the changes in droplet diameter for Sample 1(2) and Sample 4 formed in the squeezing regime

with variations in the flow rates of the dispersed and continuous phases and the capillary number of the continuous phase. A decrease in droplet size is evident due to a reduction in interfacial tension while comparing Fig. 10a, b at a fixed flow rate ratio. The size of the droplets decreases as the flow rate ratio and capillary number of the continuous phase increases. This relationship can be described using a power-law equation with a negative exponent the squeezing regime. For this regime, the droplet size can be scaled with the flow rate ratio and the capillary number of the continuous phase according to previous studies Xu et al. (2008). The drops diameter could be described by the equation: $D/D_H = \alpha(Q_c/Q_d)^\beta Ca_c^\gamma$ Liu and Zhang (2011). Our resulting equations are listed in Table 5.

For illustrative purposes, Fig. 11 showcases the droplet formation behavior for Sample 2 and Sample 4. The figures display images of the numerical simulation of droplet formation alongside the associated experimental image of on-chip collected emulsion. The production of droplets is observed in the squeezing regime, aligning with expectations.

A clear demonstration of the influence of the flow rate ratio on droplet formation is evident when comparing Fig. 11a, b. This observation holds for Fig. 11a compared to Fig. 11b, where the flow rates Q_d and Q_c are both set to 1 μL/min. Furthermore, a comparison between Fig. 11a and Fig. 11c reveals that the introduction of a surfactant in the dispersed phase results in a significant reduction in droplet size.

Based on both numerical and experimental results, it was observed that the microfluidic flow-focusing device demonstrated the capability to produce droplets with a coefficient of variation (CV) lower than 5% when operated under the squeezing regime.
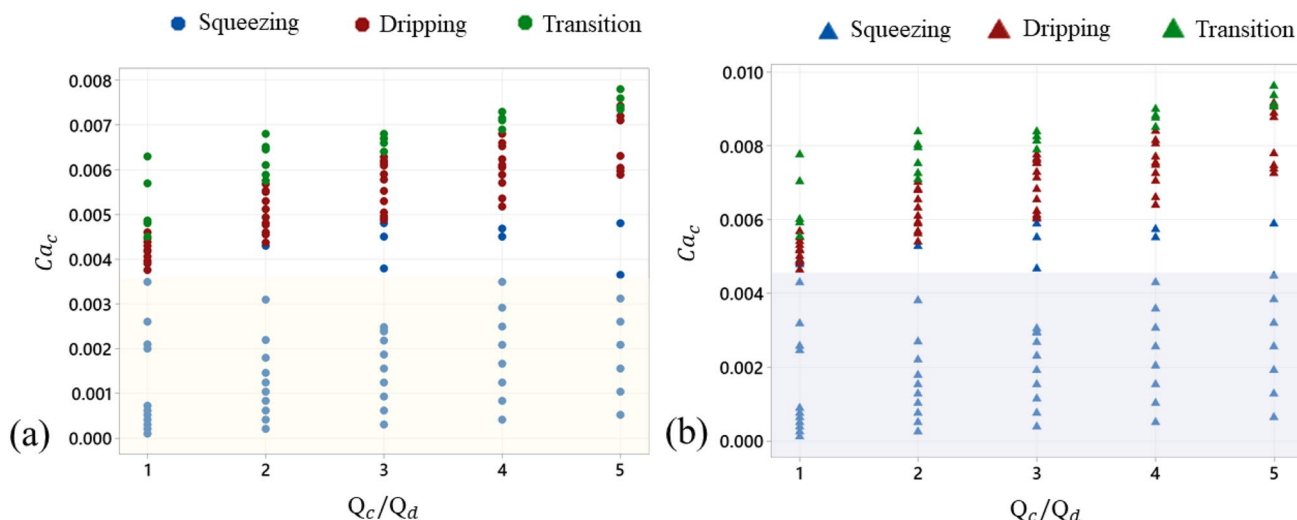
Fig. 9 Effects of flow rate ratio of two phases and capillary number of the continuous phase on flow regime map of (**a**) Sample 1 (**2**) and, (**b**) Sample 4

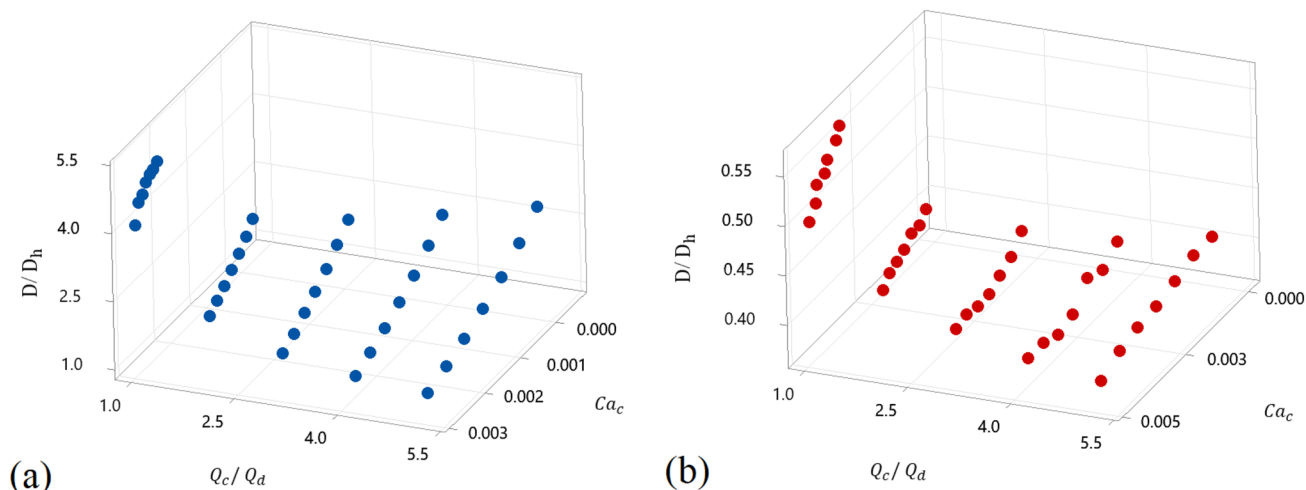**Fig. 10** Droplet diameter as a function of Ca_c and specified range of Q_c to Q_d. The droplet formation regime is found to be **a** Squeezing for Sample 1 and 2, and **b** Squeezing for Sample 4

Table 5 For distinct samples, the flow rate ratio of both phases and the capillary number of the continuous phase can be scaled

	Sample 1 (2)	Sample 4
Regime	Squeezing	Squeezing
D/D_H	$0.04(Q_c/Q_d)^{-0.65}Ca_c^{-1.16}$	0.09
		$(Q_c/Q_d)^{-0.19}$
		$Ca_c^{-1.52}$

3.2 Fractional factorial design results

To understand the impact of SDS concentration (factor A),

Span 80 concentration (factor B), and flow rate ratio (factor C) on the stability (p(1)) of a single emulsion created using the microfluidic approach, we employed a two-level, full-factorial design (2^3). To mitigate potential effects from alterations in channel properties due to repeated usage, a fresh microfluidic device was used for each sample. In our experimental setup, we established a flow rate ratio range from 1 to 5, with the dispersed phase flow rate maintained at 5 µL/min.

Emulsions created under the eight experimental settings exhibited an average geometric diameter ranging from 10.4 µm to 202.4 µm. Each case in the experimental inquiry showed no on-chip coalescence after droplet production, with a coefficient of variation (CV) consistently smaller

Fig. 11 Side-view results of numerical simulation of droplet formation and corresponding on-chip experimental results of generated droplets with Q_c= 1 μL/min (**a**) Sample 2 at Q_c/Q_d= 1 with average size of 157.1 μm (Scale bar = 80 μm), **b** Sample 2 at Q_c/Q_d= 2 with average size of 119.8 μm (Scale bar = 80 μm), and **c** Sample 4 at Q_c/Q_d= 1 with average size of 23.4 μm (Scale bar = 8 μm). In all cases, no on-chip coalescence is seen. **d** A 2D flow-focusing channel is schematic with the outlet section highlighted
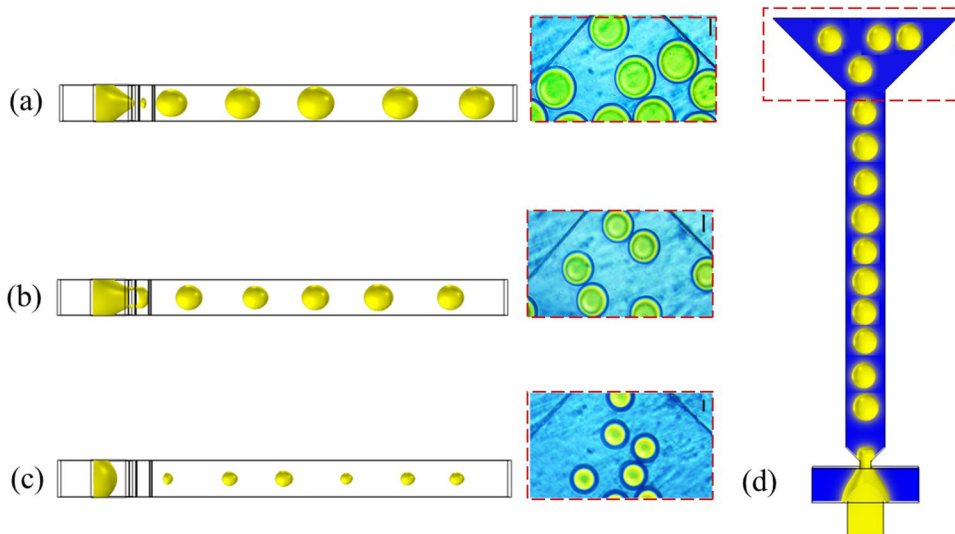

**Table 6** The experimental values of the dependent variable (stability) for each independent variable

RunOrder	StdOrder	Sample	Q_c/Q_d	Mean diameter D (μm)	Stability p(1)
1	5	3	5	135.1	0.36
2	8	4	5	10.4	0.98
3	2	2	1	146	0.51
4	4	4	1	30.5	0.95
5	7	1	5	50.1	0.65
6	6	2	5	95.3	0.56
7	3	1	1	120.8	0.45
8	1	3	1	202.4	0.25

than 5%. However, documented occurrences of coalescence were noted within the storage vessel during the process of preserving droplets, emphasizing the need for further investigation into the long-term stability of these droplets. The diameter of droplets was measured through on-chip monitoring, and the examination of coalescence phenomena was conducted 14 days after the collection process using optical observation techniques.

The effects of experimental variables on the size and stability of the emulsion are detailed in Table 6. The term "StdOrder" or standard order refers to an index utilized in creating designs with consistent run parameters. Fig. 12 depicts the emulsion immediately after its formation in the output channel and its state after two weeks in the collection container for both Sample 2 and Sample 4, with flow rate ratios set to 5 and 1, respectively. The graphic effectively illustrates the observable impact of introducing surfactant in both the continuous and dispersed phases. A comparison between the two images reveals a decrease in the flow rate ratio to one-fifth of its value in Fig. 12a, which is expected to increase in droplet size. However, the evident reduction in size can be attributed to the use of surfactant in both phases. In this context, our objective is to comprehend the

Fig. 12 Generated droplets of RunOrder **a** 6 **b** 4 and their corresponding collected emulsion (Scale bar: 100 μm.)
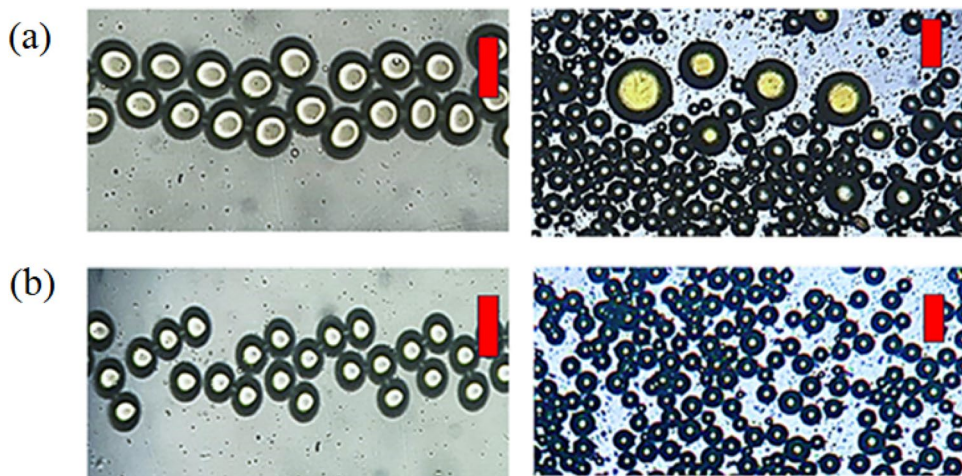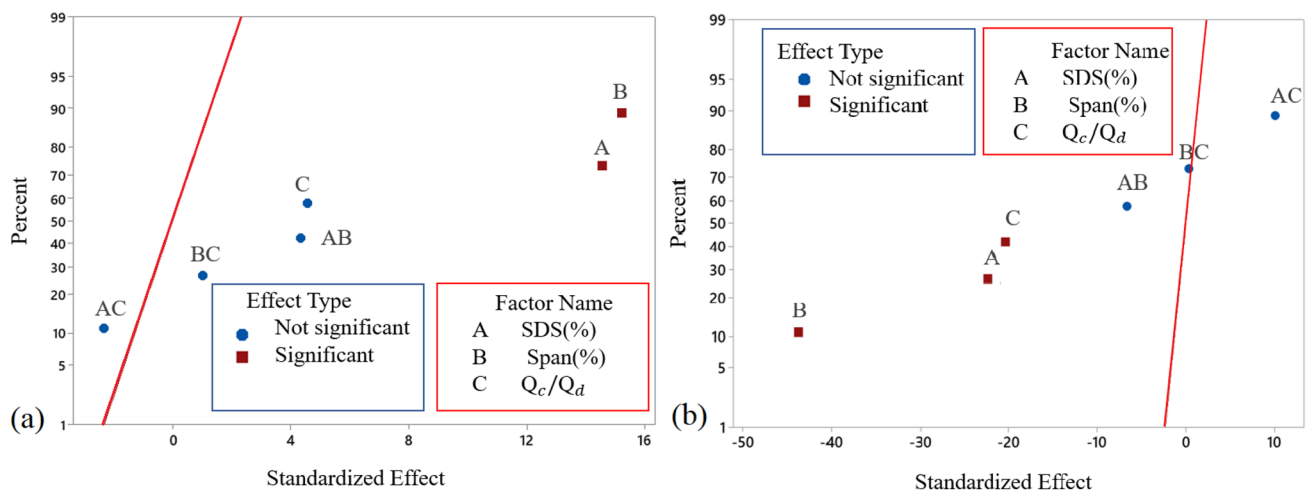
Fig. 13 Normal probability plot of the standardized effect on **a** Stability, **b** Diameter of the emulsion

importance of these variables in the size and stability of the emulsion.

The normal probability plot of the effects on stability and diameter is shown in Fig. 13. Effects that are farther away from 0 on the normal probability plot are statistically significant at the 0.05 level. When two-way interactions are included, the fitted model, an algebraic representation of the regression model, describing the influence of variables on stability is Eq. 13 C_{SDS} symbolizes the SDS concentration in percent in the aqueous phase, and C_{Span} represents the Span 80 concentration in the oil phase. (Eq. 14) is the reduced fitted model by only including significant variables which are the main effects according to Fig. 13a and Fig. 13b. For stability, the model accounts for 99.8% (R-sq = 99.8%) which demonstrates that the model fits the data well. The model's prediction ability is likewise satisfactory as the predicted R-sq is equal to 96.95%. Factors A and B significantly affect the stability of the emulsion, according to this model (P values of 0.005 and 0.004, respectively).

In Sample 3, it is observed that droplet formation does not take place at the junction. However, our experimental analysis reveals that monodisperse droplets with a mean size ranging from 135.1 µm to 202.4 µm are created at the output of the microfluidic chip, for flow rate ratios of 1 and 5, respectively. Hence, employing a minimal concentration of surfactants in both phases will result in the absence of droplet breakage at the junction. Droplet creation occurs when two parallel flows emerge from the microfluidic chip.

The results of the factorial analysis indicated that the concentration of the oil-soluble emulsifier played a significant role in determining the stability of the emulsion. Furthermore, it was observed that the water-soluble emulsifier exhibited greater efficacy in stabilizing the emulsion when compared to the flow rate ratio. The utilization of the applied fractional factorial design approach facilitated the identification of the ideal concentrations of the surfactants, along with the flow rate ratio, to create W/O emulsions with the appropriate size and stability.

Figure 14 displays contour plots illustrating the relationship between stability and two out of the three independent variables, while the other variable is held constant. Based on the analysis of the coefficient magnitudes in the fitted models, it was inferred that the stability is influenced by the Span and SDS concentration variables. The attainment of the highest emulsion stability requires the utilization of surfactants in both the continuous and dispersed phases. In contrast, when a surfactant is applied solely to one of the phases, the stability can be enhanced to a level exceeding 0.8 by raising the flow rate ratio. The concentration of SDS and Span, as well as the flow rate ratio, all exhibit a positive effect on stability. However, conversely, they all have a reductive impact on droplet diameter. The data presented in the Fig. 14 demonstrates that having the maximum concentration of both surfactants in both phases or attaining the maximum concentration of either SDS or Span 80, together with the highest flow rate ratio, leads to the smallest emulsion size. Given that the interaction effects are not statistically significant, they have been omitted from the contour plots depicting the influence of effective parameters on droplet size and emulsion stability.

There exists a clear correlation between the degree of monodispersity and stability. Emulsions that demonstrate minimum change in size following storage generally possess the highest level of stabilization. Sample 4, which exhibits the highest stability among the emulsions tested, maintains a coefficient of variation (CV) of 4.6% after a 14-day preservation period. In contrast, the remaining samples see a decline in monodispersity, accompanied by a fall in stability.

Fig. 14 Contour plot of stability versus **a** Span 80 and SDS concentration with hold value of $Q_c/Q_d = 3$, **b** SDS concentration and Q_c/Q_d with hold value of Span concentration = 1%, **c** Span concentration and Q_c/Q_d with hold value of SDS concentration = 0.1% and Contour plot of droplet diameter versus **d** Span 80 and SDS concentration with hold value of $Q_c/Q_d = 3$, **e** SDS concentration and Q_c/Q_d with hold value of Span concentration = 1%, **f** Span concentration and Q_c/Q_d with hold value of SDS concentration = 0.1%
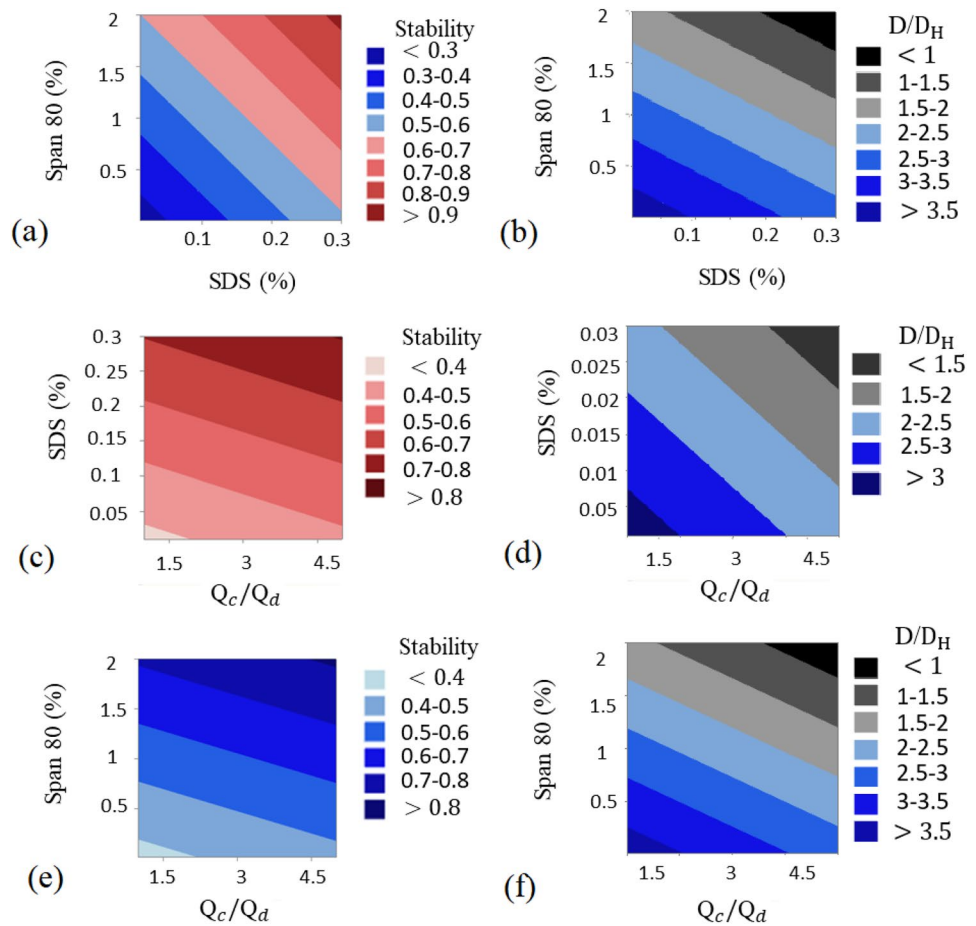
$$P(1) = 0.1940 + 1.061 C_{SDS}$$
$$+ 0.1028 C_{Span} + 0.0340 Q_c/Q_d$$
$$+ 0.3379 C_{SDS} * C_{Span} - 0.0905 C_{SDS} * Q_c/Q_d \quad (13)$$
$$+ 0.00565 C_{Span} * Q_c/Q_d$$

$$P(1) = 0.1664 + 1.129 C_{SDS}$$
$$+ 0.1721 C_{Span} + 0.0256 Q_c/Q_d \quad (14)$$

Given our confidence in the uniformity of our initial emulsion, there is no destabilization mechanism resulting from Ostwald ripening. Our primary focus is on ensuring stability against coalescence, as emphasized in Bibette et al. (1992). The importance of the emulsifier's kind and concentration in this setting is clear from our findings and has been emphasized by previous studies (Ho et al. 2022; Mcclements 2007). The enhanced stability observed with increasing surfactant concentration can be attributed to a higher quantity and density of surfactant molecules adhering to the oil–water interface. This augmentation results in a more robust and thicker film at the interface, thereby preventing coalescence, as discussed by Zhang et al. (2021). It is crucial to keep in mind that the concentration of surfactants should be kept below the critical micelle concentration (CMC), as within this range, increasing the amount of surfactant leads to a decrease in interfacial tension. Our investigation identified the flow rate ratio as an additional factor influencing emulsion stability. As previously established in Sect. 3.2, the flow rate ratio is proportional to the size of the emulsion. This conclusion aligns with the understanding that reducing the emulsion size enhances stability. Equation 14 incorporates a positive sign for the flow rate ratio, reflecting the fact that larger aggregates separate at a faster rate than smaller individual droplets.
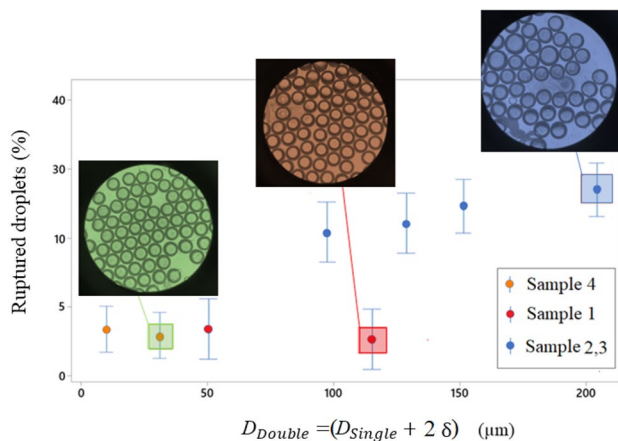
Fig. 15 Percentage of ruptured double droplets versus mean diameter of double emulsion which is the sum of single emulsion and shell thickness for different samples. Visual representations of Sample 4, Sample 2, and Sample 3 are included

4 Single-core double emulsion

To explore the impact of the initial single emulsion on the resulting double emulsion, the process of re-emulsification is repeated for all eight samples under examination. Consistency in the outer phase and vortexing conditions across all samples is expected to result in uniform shell thickness, as indicated in previous studies by Wang et al. (2022), Lin et al. (2022). It is crucial to note that the surfactant present in the external phase (DI water and 0.3% SDS) remains constant throughout the entire experiment.

The shell thickness, represented as δ (mean difference of oil droplet diameter and outer water droplet diameter), is a key parameter. Figure 15 illustrates the relationship between the average size of the double emulsion and the corresponding percentage of ruptured double emulsions for each sample. The graphic depictions in Fig. 15 indicate the absence of individual water droplets in the receptacle, suggesting that the discharge of the internal core has not occurred. Additionally, the infrequent or lack of observed augmentation in the inner water phase droplet implies that the fusion of water cores did not transpire in our specific experiments Leister and Karbstein (2023).

For double emulsions made from samples 2 and 3, which have no Span 80 in the oil phase, there is an average rupture rate of 11.3%. This behavior is less frequently observed in double emulsions of samples 1 and 4. Both of these samples exhibit the common feature of having a 2% concentration of Span 80 in the oil phase. The stability of the double emulsion can be ascribed to the surfactant present in the oil phase. In the context of a double emulsion of water-in-oil–water, it is justified to disregard the interfacial interactions related to the water core and treat the system as an oil-in-water emulsion. This is anticipated because Eq. 13

states that the primary factor of importance is the concentration of surfactant in the inner phase, which corresponds to the oil phase in this particular scenario. In the specific case of w/o/w fabrication, the stability of the double emulsion is regulated by the surfactant Span 80, contained in the oil phase of the emulsion.

A key use of double emulsion generation is to create microcapsules comprising of an aqueous core and a polymeric shell. The eight preexisting samples are re-emulsified using a vortex mixer and stirred for 16 h to expedite the volatilization of the volatile solvent (DCM) and the consequent creation of solid microparticles. According to Fig. 16a, the production of microparticles with a coefficient of variation (CV) of less than 3% is achieved when the value of P(1) is greater than 0.9. The diameter of corresponding single emulsion droplets in this scenario is smaller than 50 micrometers. Moreover,r we want to show using our correlation, one may generate microparticles of the desired size and uniformity under full control. As an illustration, the size of single emulsion droplets is adjusted to a specific diameter of 50 microns, while their capacity to remain stable is adjusted to a desirable level of 95% in the obtained equations, Eq. 13 and Table 3. These equations provide the following values as the operating conditions: $Q_c/Q_d = 2.5$, concentration of Span 80 in the oil phase containing PLGA in DCM and mineral oil = 2%, and concentration of SDS in the inner aqueous phase = 0.3%. The stable single emulsion, with an average diameter of 50 μm, is subjected to re-emulsification in an aqueous phase containing 0.3 wt% SDS. The re-emulsification procedure resulted in the successful production of single-core double emulsions, characterized by an average shell thickness of 4 microns. The coefficient of variance in shell thickness was found to be 3%. The experiment was conducted in triplicate to ensure the reliability of the findings which are demonstrated in Fig. 16b. The final average size of microparticles after size reduction due to solvent evaporation is 16.9 μm with CV = 2.9%.

5 Conclusion

Microfluidic devices are well-known for making extremely monodispersed emulsions of the desired size; nevertheless, maintaining the emulsion without losing monodispersity is a challenge for which we are seeking a solution. The purpose of this research is to investigate the long-term durability and size management of microfluidic-produced single emulsions with high monodispersity immediately after fabrication. While our numerical analysis did not provide direct stability measurements, it empowered us to make informed estimations regarding the stability of single emulsions. We prepared four oil and water phase samples, each with varying concentrations to produce distinct interfacial tension

Fig. 16 Double emulsion made from single emulsion with size of 50 μm and the resulting microparticle after solvent evaporation with average size of 16.9 μm
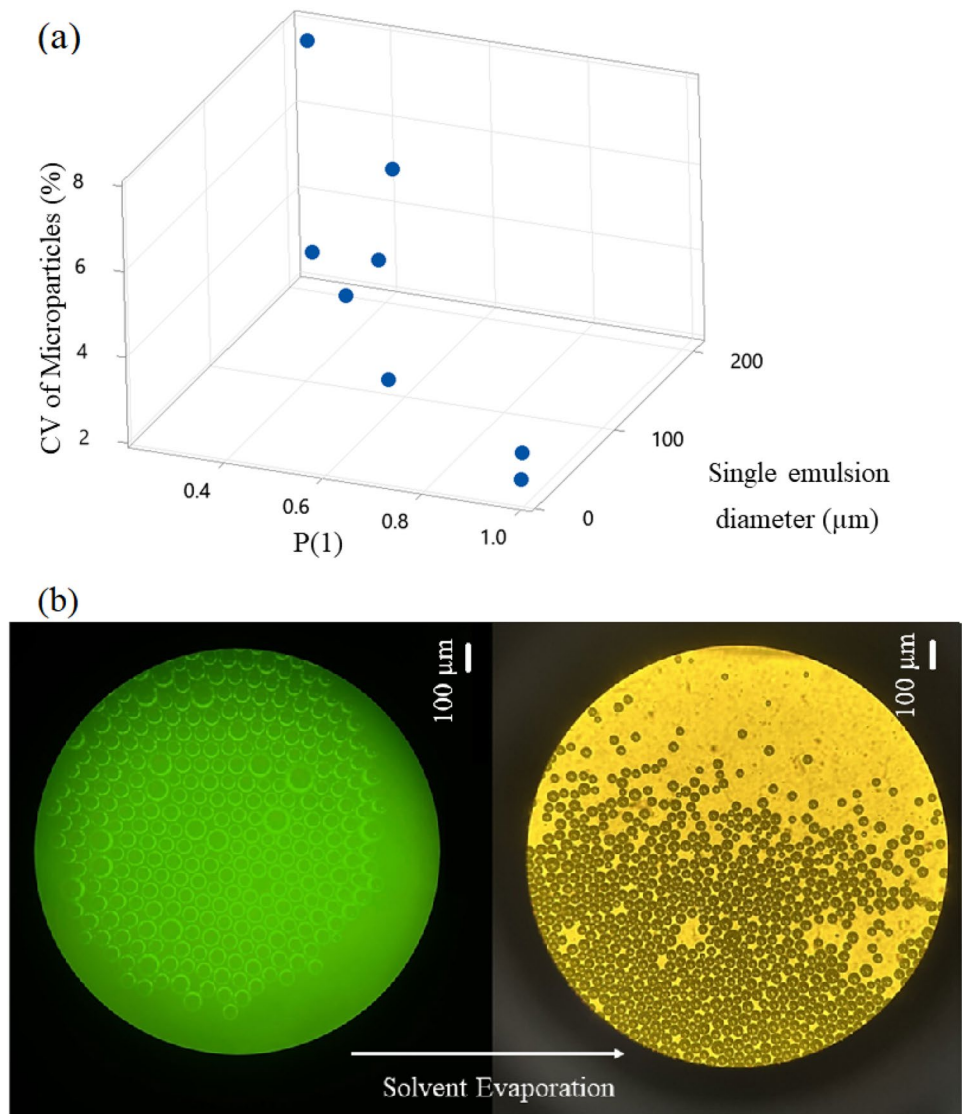
from 1.7 mN/m to 30.5 mN/m. Initially, we utilized validated numerical simulation employing the level-set approach to ascertain the necessary flow rate ratio and capillary number of the continuous phase to generate droplets of each sample within the squeezing regime. The selection of this regime was made to generate uniform droplets while ensuring that there is no variation in droplet size caused by the microfluidic droplet fabrication process. The coefficient of variation in the size of produced droplets is consistently below 5% when measured on-chip. To understand how different factors such as surfactant concentration and flow rate ratio affect the long-term stability of an emulsion, which refers to its capacity to maintain the uniform distribution of droplets, a fractional factorial design is employed to establish a correlation.

To summarize our findings, we can emphasize these conclusions:

1. Under the conditions of the squeezing regime, to facilitate emulsion size predictions, we offer correlations based on numerical results. The emulsion size is a function of the flow rate ratio and the capillary number of the continuous phase. However, the magnitude of the exponent of each variable varies depending on the interfacial tension, which is influenced by the concentration of surfactants. The exponents are estimated for each case in our study.

2. The numerical simulation results are more accurate when the drop in interfacial tension is achieved by adding surfactants to the continuous phase rather than the dispersed phase.

3. Based on the fractional factorial design results, it becomes evident that an increase in the flow rate ratio and the elevation of surfactant concentration within the specified range are key drivers of emulsion size reduction and improved stability. In our special case,

with maximum magnitude (98%) of flow rate ratio and having surfactants in both water and oil phases.

4. By ensuring that the operating regime is the squeezing regime, one may utilize our established models to forecast the size of droplets and the stability of the created emulsion. This can be done by knowing the concentrations of oil-soluble and water-soluble surfactants, as well as the flow rate ratio.

In the concluding phase of our investigation, we employed a vortex to re-emulsify the single emulsion, resulting in the formation of a single core water-in-oil-in-water emulsion. We reveal that the stability of re-emulsified water-in-oil emulsions is primarily dictated by the concentration of surfactant within the oil phase since without surfactant in the oil phase, rupture of the emulsion is observed in 11.3% of the cases. Our findings indicate that the stability of re-emulsified water-in-oil emulsions is mostly determined by the surfactant concentration in the oil phase. In circumstances where there is no surfactant present in the oil phase, emulsion rupture occurs in 11.3% of instances. Our objective was to create microparticles by volatile solvent evaporation. A single emulsion with an arbitrary size of 50 microns and a stability of 95% is demanded. By analyzing the correlation we acquired, we determined the necessary concentration of surfactant and the ratio of flow rates to produce this emulsion. After successfully creating the double emulsions, we allowed the volatile solvent in the oil phase to evaporate, resulting in the formation of solid microparticles of 16.9 μm.

In conclusion, our research contributes to the evolving field of emulsion science, offering a robust framework for predicting and controlling the long-term behavior of emulsions. These findings hold great promise for various industries and researchers seeking to harness the potential of emulsions for a wide array of applications, ranging from pharmaceuticals to food technology and beyond.

Declarations

References

Abdulredha MM, Hussain SA, Abdullah LC (2019) Separation emulsion via non-ionic surfactant: an optimization. Processes 7(6):382

Ait-Amir B, Pougnet P, El Hami A (2020) Meta-model development. In: Embedded Mechatronic Systems 2, pp. 157–187. Elsevier

Baret J-C, Kleinschmidt F, El Harrak A, Griffiths AD (2009) Kinetic aspects of emulsion stabilization by surfactants: a microfluidic analysis. Langmuir 25(11):6088–6093

BenJemaa M, Rahali FZ, Falleh H, Beji-Serairi R, Megdiche-Ksouri W, Hamrouni I, Hammami M, Nehme R, Pereira RB, Andrés S et al (2022) Essential oil stabilisation by response surface methodology (rsm): nanoemulsion formulation, physicochemical, microbiological, and sensory investigations. Molecules 27(21):7330

Bibette J, Morse D, Witten T, Weitz D (1992) Stability criteria for emulsions. Phys Rev Lett 69(16):2439

Brackbill JU, Kothe DB, Zemach C (1992) A continuum method for modeling surface tension. J Comput Phys 100(2):335–354

Chacon Orellana LA, Baret J-C (2019) Rapid stabilization of droplets by particles in microfluidics: role of droplet formation. Chem Syst Chem 1(1–2):16–24

Chagot L, Quilodrán-Casas C, Kalli M, Kovalchuk NM, Simmons MJ, Matar OK, Arcucci R, Angeli P (2022) Surfactant-laden droplet size prediction in a flow-focusing microchannel: a data-driven approach. Lab Chip 22(20):3848–3859

Chatterjee A, Moulik S, Sanyal S, Mishra B, Puri P (2001) Thermodynamics of micelle formation of ionic surfactants: a critical assessment for sodium dodecyl sulfate, cetyl pyridinium chloride and dioctyl sulfosuccinate (na salt) by microcalorimetric, conductometric, and tensiometric measurements. J Phys Chem B 105(51):12823–12831

Chen Y, Narayan S, Dutcher CS (2020) Phase-dependent surfactant transport on the microscale: interfacial tension and droplet coalescence. Langmuir 36(49):14904–14923

Colucci G, Santamaria-Echart A, Silva SC, Fernandes IP, Sipoli CC, Barreiro MF (2020) Development of water-in-oil emulsions as delivery vehicles and testing with a natural antimicrobial extract. Molecules 25(9):2105

Dapčević Hadnađev T, Dokić P, Krstonošić V, Hadnađev M (2013) Influence of oil phase concentration on droplet size distribution and stability of oil-in-water emulsions. Eur J Lipid Sci Technol 115(3):313–321

El Bouchikhi S, Ibrahimi A, Bensouda Y et al (2021) Creaming behavior prediction of argan oil in water emulsion stabilized by lacto-fermentation: creaming index. BMC Biotechnol 21(1):1–11

Filimonov R, Wu Z, Sundén B (2021) Toward computationally effective modeling and simulation of droplet formation in microchannel junctions. Chem Eng Res Design 166:135–147

Francisco CRL, Santos TP, Cunha RL (2022) Design of shear-based microfluidic channels for production and stability assessment of food emulsions. Curr Opin Food Sci:100957

Fu T, Wu Y, Ma Y, Li HZ (2012) Droplet formation and breakup dynamics in microfluidic flow-focusing devices: from dripping to jetting. Chem Eng Sci 84:207–217

Goodarzi F, Zendehboudi S (2019) A comprehensive review on emulsions and emulsion stability in chemical and energy industries. Canad J Chem Eng 97(1):281–309

Ho TM, Razzaghi A, Ramachandran A, Mikkonen KS (2022) Emulsion characterization via microfluidic devices: a review on interfacial tension and stability to coalescence. Adv Coll Interface Sci 299:102541

Issakhani S, Jadidi O, Farhadi J, Bazargan V (2023) Geometrically-controlled evaporation-driven deposition of conductive carbon nanotube patterns on inclined surfaces. Soft Matter 19(7):1393–1406

Jayakumar J, Ballon A, Pallarès J, Vernet A, Lamo-Castellví S, Güell C, Ferrando M (2023) Lesser mealworm (a. diaperinus) protein as a replacement for dairy proteins in the production of o/w emulsions: droplet coalescence studies using microfluidics under controlled conditions. Food Res Int:113100

Kiratzis I, Kovalchuk NM, Simmons MJ, Vigolo D (2022) Effect of surfactant addition and viscosity of the continuous phase on flow fields and kinetics of drop formation in a flow-focusing microfluidic device. Chem Eng Sci 248:117183

Kumar B, Tikariha D, Ghosh KK, Barbero N, Quagliotto P (2013) Effect of polymers and temperature on critical micelle concentration of some gemini and monomeric surfactants. J Chem Thermodyn 62:178–185

Leister N, Karbstein HP (2023) Determination of the dominating coalescence pathways in double emulsion formulations by use of microfluidic emulsions. Processes 11(1):234

Lin S, Mao L, Ying J, Berthet N, Zhou J, Riaud A (2022) Generation of double emulsions from commercial single-emulsion microfluidic chips: a quality-control study. Microfluid Nanofluid 26(9):71

Liu H, Zhang Y (2011) Lattice boltzmann simulation of droplet generation in a microfluidic cross-junction. Commun Comput Phys 9(5):1235–1256

Liu Z, Chai M, Chen X, Hejazi SH, Li Y (2021) Emulsification in a microfluidic flow-focusing device: effect of the dispersed phase viscosity. Fuel 283:119229

Mahdi Y, Daoud K, Tadrist L (2017) Two-phase flow patterns and size distribution of droplets in a microfluidic t-junction: experimental observations in the squeezing regime. Compt Rendus Mecanique 345(4):259–270

Mcclements DJ (2007) Critical review of techniques and methodologies for characterization of emulsion stability. Crit Rev Food Sci Nutr 47(7):611–649

Mitra SK, Chakraborty S (2012) Microfluidics and nanofluidics handbook: fabrication, implementation, and applications. Taylor & Francis

Mohd Isa N, El Kadri H, Vigolo D, Gkatzionis K (2022) The effect of bacteria on the stability of microfluidic-generated water-in-oil droplet. Micromachines 13:2067. (Note: MDPI stays neutral with regard to jurisdictional claims in published …)

Narayan S, Makhnenko I, Moravec DB, Hauser BG, Dallas AJ, Dutcher CS (2020) Microscale investigation of binary droplet coalescence using a microfluidic hydrodynamic trap. arXiv preprint arXiv: 2005.07816

Oveysi M, Zaker MA, Peregrino G, Bazargan V, Marengo M (2023) Droplet-based fabrication of alginate hydrogel microparticles in presence of surfactants. Microfluid Nanofluid 27(7):45

Paiboon N, Surassmo S, Ruktanonchai UR, Soottitantawat A (2022) Hydrodynamic control of droplet formation in narrowing jet and tip streaming regime using microfluidic flow-focusing. Int J Multiph Flow 150:104013

Raya SA, Saaid IM, Aji AQM, Razak AAA (2022) Investigation of the synergistic effect of nonionic surfactants on emulsion resolution using response surface methodology. RSC Adv 12(48):30952–30961

Sahin S, Bliznyuk O, Rovalino Cordova A, Schroën K (2016) Microfluidic edge emulsification: the importance of interface interactions on droplet formation and pressure stability. Sci Rep 6(1):26407

Sanchez SM, Sanchez PJ, Wan H (2020) Work smarter, not harder: a tutorial on designing and conducting simulation experiments. In: 2020 Winter Simulation Conference (WSC), pp. 1128–1142. IEEE

Sontti SG, Atta A (2019) Numerical insights on controlled droplet formation in a microfluidic flow-focusing device. Ind Eng Chem Res 59(9):3702–3716

Soroor M, Targhi MZ, Tabatabaei SA (2021) Numerical and experimental investigation of a flow focusing droplet-based microfluidic device. Eur J Mech B/Fluids 89:289–300

Wang J, Hahn S, Amstad E, Vogel N (2022) Tailored double emulsions made simple. Adv Mater 34(5):2107338

Wu Z, Cao Z, Sunden B (2019) Flow patterns and slug scaling of liquid-liquid flow in square microchannels. Int J Multiph Flow 112:27–39

Xu JH, Li S, Tan J, Luo G (2008) Correlations of droplet formation in t-junction microfluidic devices: from squeezing to dripping. Microfluid Nanofluid 5:711–717

Yu W, Liu X, Zhao Y, Chen Y (2019) Droplet generation hydrodynamics in the microfluidic cross-junction with different junction angles. Chem Eng Sci 203:259–284

Zdrali E, Etienne G, Smolentsev N, Amstad E, Roke S (2019) The interfacial structure of nano-and micron-sized oil and water droplets stabilized with sds and span80. J Chem Phys 150(20)

Zembyla M, Murray BS, Sarkar A (2020) Water-in-oil emulsions stabilized by surfactants, biopolymers and/or particles: a review. Trends Food Sci Technol 104:49–59

Zhang L (2014) Numerical simulation of two-phase flow using the level set approach. PhD thesis

Zhang T, Ding M, Wang X, Zhong J (2020) Droplet and creaming stability of fish oil-loaded gelatin/surfactant-stabilized emulsions depends on both the adsorption ways of emulsifiers and the adjusted ph. Food Sci Hum Wellness 9(3):280–288

Zhang J, Ge D, Wang X, Wang W, Cui D, Yuan G, Wang K, Zhang W (2021) Influence of surfactant and weak-alkali concentrations on the stability of o/w emulsion in an alkali-surfactant-polymer compound system. ACS Omega 6(7):5001–5008

Zhang T, Zhang X, Jin M, Zhang Y, Jiang L, Sui X (2023) Parameter control, characterization and stability of soy protein emulsion prepared by microfluidic technology. Food Chem:136689